Electrochimica Acta 54 (2009) 6028–6035

Contents lists available at ScienceDirect

Electrochimica Acta

journal homepage: www.elsevier.com/locate/electacta

Electrodeposition of rhenium–nickel alloys from aqueous solutions

A. Naor [a], N. Eliaz [a,*], E. Gileadi [b,1]

[a] Biomaterials & Corrosion Laboratory, School of Mechanical Engineering & The Materials Science and Engineering Program, Tel-Aviv University, Ramat-Aviv 69978, Israel
[b] School of Chemistry, Raymond and Beverly Sackler Faculty of Exact Sciences, Tel-Aviv University, Ramat-Aviv 69978, Israel

ARTICLE INFO

Article history:
Received 2 December 2008
Received in revised form 1 March 2009
Accepted 2 March 2009
Available online 17 March 2009

Keywords:
Rhenium–nickel alloy
Electrodeposition
Induced codeposition

ABSTRACT

Rhenium–nickel alloys were deposited on copper substrates in a small three-electrode cell, under galvanostatic conditions. The bath solution consisted of ammonium perrhenate, citric acid and nickel sulfamate. The effects of bath composition and deposition time were studied. The Faradaic efficiency (FE) and partial deposition current densities were calculated based on mass gain and elemental analysis using energy dispersive spectroscopy. The surface morphology was characterized by scanning electron microscopy. The thickness of the coating was measured on metallographic cross-sections. The results are discussed with emphasis on routes to increase the Faradaic efficiency and rhenium content in the coating. A plausible mechanism for the electrodeposition of rhenium–nickel alloys is presented.

1. Introduction

Rhenium (Re) differs from the other refractory metals (Nb, Ta, Mo and W) in that it has a hexagonal close-packed (hcp) structure, and does not form carbides. Its structure eliminates a ductile-to-brittle transition and allows Re to remain ductile and strong from subzero to high temperatures. It has the second highest melting point of all metals (after W), 3157–3181 °C [1], the fourth highest density (after Os, Ir and Pt), 21.00–21.02 g cm^{-3} [1], and the third highest modulus of elasticity (after Ir and Os), 461–471 GPa [1]. Rhenium is hard, 2.6–7.5 GPa [1], and has a low coefficient of friction. It also has one of the highest strain hardening exponents of all elements, 0.353 [2], giving it a high shear modulus, 155 GPa [2], and excellent wear properties. Compared with other refractory metals, Re has superior tensile strength, 1000–2500 MPa [1], and creep-rupture strength, 10 MPa for 100 h at 2200 °C [2], over a wide temperature range. The attribute ranges reflect different thermal conditions and suppliers of the commercially pure metal. At elevated temperatures, Re resists attack in hydrogen and inert atmospheres. It is also resistant to hydrochloric acid and seawater corrosion. While pure Re is vulnerable to oxidation in moist air above 600 °C due to formation of Re_2O_7 and its penetration into the grain boundaries, improvements in this and other properties are being sought through the development of Re alloys and the application of an oxidation-resistant top coating (e.g., Ir, Pt or Rh) [3].

The unique combination of properties of Re is useful in different applications, including aircraft, aerospace, nuclear, electrical, catalysis and biomedical [3]. For example, it has been considered for use in divert and attitude propulsion subsystems, e.g., as a protective coating of carbon–carbon composites, in rocket engine exhaust nozzles, etc. [4–9]. In the aircraft industry, Re is also used as an alloying element of single crystal Ni-based superalloys for turbine blades, as a coating of face seal rotors, in air turbine starter components for gas turbine engines, as a diffusion barrier (e.g., on top of graphite [10], Ni_3Al-based superalloy for vanes [11] or Nb-based alloy in advanced jet engines [12]).

Most of the published reports to-date deal with fabrication of Re-based items by chemical vapor deposition (CVD). However, CVD is an expensive, complex and energy intensive process that results in delamination-prone coated components. Electroplating at near-room temperature using non-toxic bath chemistries may become a successful alternative and also allow for uniform Re coatings on complex shapes.

Electrodeposition of Re and its alloys has recently been reviewed by Eliaz and Gileadi [3]. Rhenium belongs to a group of metals that are difficult to produce by electrolysis of their aqueous solutions, mainly because of its very low overpotential for hydrogen evolution. Its most stable form in solution is ReO_4^-, which is iso-electronic with WO_4^{2-}. However, unlike W, it can be electrodeposited from aqueous solutions as a pure metal, similar to Os, Ir and Pt, but the Faradaic efficiency (FE) is low and the resulting coating is brittle, as a result of absorbed hydrogen. The Pourbaix diagram of Re [13] indicates that both potential and pH must be finely controlled to maximize deposition of metallic Re and minimize hydrogen evolution. In addition to electrochemical control, improvements are also expected through the inclusion of alloying elements.

* Corresponding author. Tel.: +972 3 640 7384; fax: +972 3 640 7617.
E-mail address: neliaz@eng.tau.ac.il (N. Eliaz).
[1] ISE Fellow.

0013-4686/$ – see front matter © 2009 Elsevier Ltd. All rights reserved.
doi:10.1016/j.electacta.2009.03.003

It has been reported that a thick, crack-free Re-iron group metal coatings can be obtained at high FE [14]. Berezina et al. [15] also reported that deposition of pure Re from sulfamate-containing baths is characterized by low FE, which could be increased to about 43% when the bath contained even a low relative concentration of nickel (Ni(II):Re(VII) = 1:10), showing a catalytic effect of nickel deposition on the deposition of Re and its alloy. According to our own preliminary experiments, electroplating of pure Re was associated with low FE (≤7%) and resulted in poor coating quality. Thus, this paper focuses on electrodeposition of Re–Ni alloys. This system has already been studied before to some extent (see, for example, [15–21]). The metallurgical interest in this system stems from the extensive mutual solubility of Re and Ni, the absence of intermetallic compounds in the Re–Ni phase diagram, and the less brittle character of Re–Ni compared to pure Re and even to Re–Co alloys. The goals of this work are to enhance the understanding of the mechanisms that control the co deposition of Re–Ni alloys and to improve the process so that high-quality coatings can be produced at acceptable FE.

2. Experimental

2.1. Plating bath chemistry

Rhenium–nickel alloys were electroplated from aqueous solutions containing 34–93 mM NH_4ReO_4 (ammonium perrhenate, Sigma–Aldrich #316954), 34–124 mM $Ni(NH_2SO_3)_2{\cdot}4H_2O$ (nickel(II) sulfamate tetrahydrate, Aldrich Chemical #26,227-7) and 34–343 mM $C_6H_8O_7$ (citric acid, Frutarom #878591) as the complexing agent. All components were dissolved in deionized water (Simplicity™, Millipore). All of the experiments were conducted at pH = 5.0 ± 0.1. The pH was measured by means of InoLab pH/Oxi Level 3 meter from WTW and adjusted at room temperature to the desired value by additions of NaOH, and in some cases small amounts of H_2SO_4. No additives were used. The conductivity of the solution was 10–20 mS cm^{-1}. The volume of electrolyte in the cell was about 10 mL. Each experiment was conducted in a fresh solution.

Nickel sulfamate is a salt of the strong monobasic sulfamic acid (NH_2SO_3H). Its incorporation in nickel (and other) plating baths has been reported to result in higher deposition rates attainable, superior throwing power, as well as reduced porosity and reduced residual stresses in the deposit [22]. Citric acid is a commonly used complexing agent. It is a tri-basic acid, which deprotonates gradually as the pH is increased. At pH = 5.0 ± 0.1, correcting for the activity and the temperature, the main species in solution are H_2Cit^- (11.6%), $HCit^{2-}$ (67.7%) and Cit^{3-} (20.7%), cf. Fig. 6.

2.2. Operating conditions

In this work, a small three-electrode cell was used. A sheet of copper with an exposed area $A = 1.57\ cm^2$ was used as the working electrode. Preliminary studies revealed no significant difference between the deposition characteristics on copper vs. gold substrates. Two platinum sheets were used as the anodes, and were placed at about 0.5 cm away from both sides of the cathode. The diameter of the counter electrode was 20% smaller than that of the working electrode.

A Princeton Applied Research model 263A Potentiostat/Galvanostat was used to control the applied current density at 50 mA cm^{-2}. It was reported that increase of the current density above this value could lead to spongy deposits [17] and almost halved the Re content in the deposit [15].

The FE was calculated from the mass gained, the charge passed and the chemical composition of the deposit, as determined by energy dispersive spectroscopy (EDS). It was calculated using the equation:

$$\mathrm{FE} = \frac{w}{It}\sum\frac{c_i n_i F}{M_i} \times 100 \quad (1)$$

where w is the measured weight of the deposit (g), t is the deposition time (s), I is the total current passed (A), c_i is the weight fraction of the element (either Re or Ni) in the binary alloy deposit, n_i is the number of electrons transferred per atom of each metal (n_i = 7 and 2 for Re and Ni, respectively), M_i is the atomic mass of that element (M_i = 186.2 and 58.71 g mol^{-1} for Re and Ni, respectively) and F is the Faraday's constant (96,485 C $equiv^{-1}$).

The partial deposition current densities were calculated from the mass gained and the chemical composition of the deposit, as determined by EDS, using the equation:

$$i_i = \frac{w}{At}\frac{c_i n_i F}{M_i} \quad (2)$$

where i_i is the partial current density of element i and A is the surface area of the cathode (cm^2).

The bath was purged with pure nitrogen for about 15 min before turning on the current. Nitrogen was passed above the solution during deposition. In all cases, the plating bath was operated at a temperature of 70 ± 0.01 °C. A Lauda Ecoline E-220T thermostatic bath was employed to control the temperature. Stirring was applied in order to maintain the homogeneity of solution and reduce pitting that could be caused by accumulation of hydrogen bubbles at the surface of the cathode [22]. The rotating speed of the magnetic stirring bar was set at 500 rpm. The electroplating process was typically run for 1 h, but the shortest experiment time was 20 min.

2.3. Characterization techniques

The surface morphology of the deposits after drying was observed by means of an environmental scanning electron microscope operated in the high vacuum mode (ESEM, Quanta 200 FEG from FEI). The attached liquid-nitrogen-cooled Oxford Si EDS detector was used to determine the atomic composition of the alloy. Each sample was analyzed at five locations, to confirm uniformity. Metallographic cross-sections of selected samples were prepared in order to characterize the coating thickness and uniformity. The thickness of selected coatings was measured on metallographic cross-sections by means of analySIS Docu image analysis package. The backscattered electrons images for these measurements were acquired under the low-vacuum mode. The hardness of the coating was measured on a metallographic cross-section at 23 °C by means of a CSM Nano Indentation Tester (NHT), using a Berkovich-type indenter.

3. Results

In the framework of this study, more than 60 samples were coated under different bath chemistries and operating conditions and subsequently characterized. In Section 3.1, the effects of the analytical concentration of nickel, citrate and perrhenate on the FE, partial currents densities and rhenium content in the deposited alloy are shown. Subsequently, Section 3.2 describes the effects of time on the FE, partial deposition current densities and rhenium content. Finally, the surface morphology and thickness of representative coatings are analyzed in Section 3.3.

3.1. The effect of the perrhenate, nickel and citrate concentrations in the bath

In Section 2.1 it was noted that all plating baths consisted of NH_4ReO_4, $Ni(NH_2SO_3)_2$ and $C_6H_8O_7$. Fig. 1a shows the effect of the

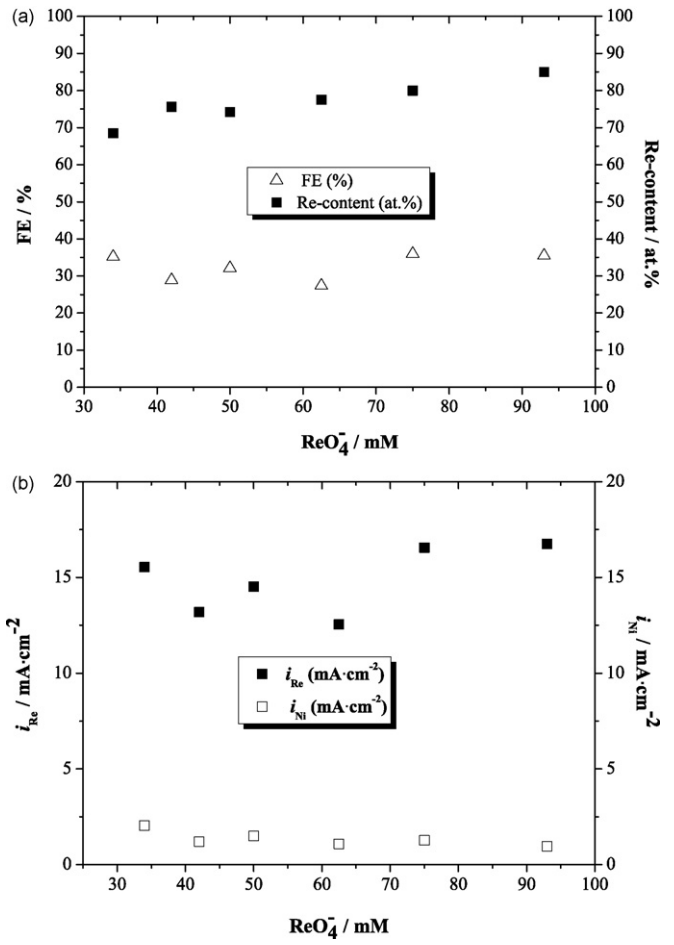

Fig. 1. (a) Dependence of the FE and the Re-content in the deposit on the analytical concentration of ReO_4^-. (b) The partial current densities of Ni and Re deposition, as a function of the analytical concentration of ReO_4^-. The analytical concentrations of Ni^{2+} and citric acid were 93 mM and 343 mM, respectively. Plating was conducted for 1 h, at 70 °C and 50 mA cm^{-2}, pH = 5.0 ± 0.1.

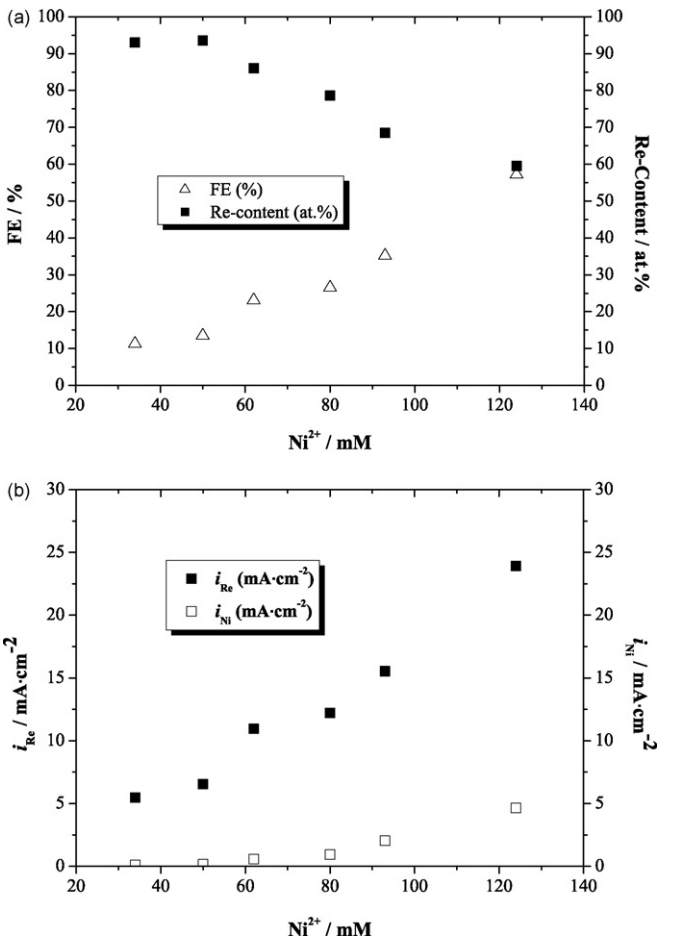

Fig. 2. Same as Fig. 1, but plotted here as a function of the analytical concentration of Ni^{2+} in solution. The ReO_4^- and citric acid analytical concentrations were 34 mM and 343 mM, respectively.

ReO_4^- concentration on the FE and Re content. The dependence of the partial current densities of Re and Ni on the concentration of the ReO_4^- ion are shown in Fig. 1b. In both cases, the concentrations of the Ni^{2+} and citric acid in the bath were 93 mM and 343 mM, respectively. The FE is seen to be essentially independent of the concentration of ReO_4^-, while the Re content increased from 69 to 85 a/o (at.%), over the range of ReO_4^- concentration shown in Fig. 1a. Fig. 1b shows that the partial current density for Re increased and that for Ni decreased with increasing concentration of ReO_4^-.

Fig. 2 shows the same quantities, but plotted here as a function of the concentration of Ni^{2+} ions in solution. The concentrations of ReO_4^- and citric acid in the bath were 34 mM and 343 mM, respectively. The FE increases steadily with increasing Ni^{2+} concentration, while the Re content decreases in the same range. It should be noted that, although the Re-content of the alloy decreases, the partial current density for Re increases with increasing concentration of Ni^{2+}, showing a catalytic effect of Ni^{2+} on the rate of deposition of Re, as will be discussed below.

The effect of the citric acid concentration on the FE, Re-content in the deposit, and partial currents densities was studied, as shown in Fig. 3. The FE decreased as the citrate-to-nickel ratio was increased. In Fig. 3a, one should note the very high FE (96%) that was obtained at the lowest concentration of citric acid.

The Re-content of the alloy showed a somewhat complex behavior: it was 33 and 59 a/o at the lowest citric acid concentration (where FE = 75% and 96%, respectively), then decreased with increasing concentration of citric acid, going through a minimum at citrate/nickel ≈ 1, and increased again to 69 and 79 a/o at the highest value of the citrate-to-nickel ratio. This behavior will be treated in the discussion section. Suffice to say here, there seems to be a correlation between decreasing FE and increasing Re-content.

The dependence of the partial current densities of Re and Ni deposition on the citrate-to-nickel ratio is shown in Fig. 3b. The behavior in this figure is complex, similar to the complexity of the Re-content shown in Fig. 3a. The partial current density i_{Re} shows a minimum, and correspondingly i_{Ni} exhibits a maximum, when the ratio of citrate-to-nickel is about unity. When viewing the partial current densities for Ni and Re it should be borne in mind that deposition of Re requires seven electrons, while that of Ni requires only two electrons.

3.2. The effect of time

The effect of operating time on the FE, Re-content in the deposit and partial deposition current densities was investigated for a bath containing 93 mM $Ni(NH_2SO_3)_2$, 34 mM NH_4ReO_4 and 343 mM citric acid. No significant effect was observed for operating times between 20 and 100 min. The FE was maintained at about 35–39%, the Re-content in the deposit was 66∼71 a/o, and the partial deposition currents of Re and Ni were 16–17 mA cm^{-2} and 2–3 mA cm^{-2}, respectively. The mass gain showed a linear dependence on time. A plot of the weight gain Δm *vs.* time yielded a deposition rate of 17.5 ± 2 mg cm^{-2} h^{-1}.

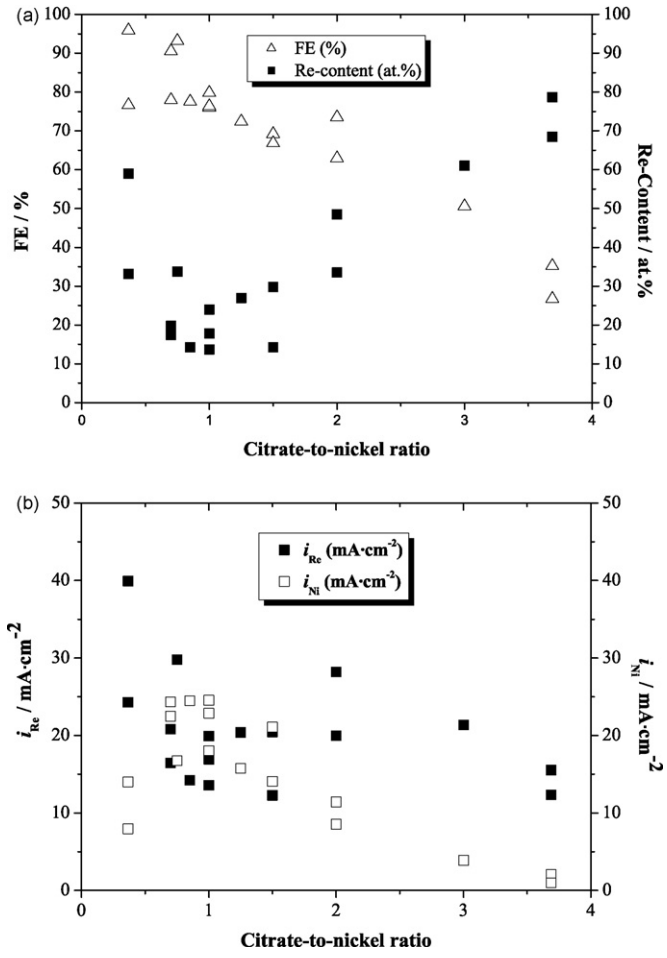

Fig. 3. Same as Fig. 1, but plotted here as a function of the analytical concentration of citric acid. The NH_4ReO_4 and $Ni(NH_2SO_3)_2$ concentrations were 34 mM and 93 mM, respectively.

3.3. Surface morphology and thickness

The surface morphology of the "as-deposited" samples and their approximate chemical composition were studied by ESEM and EDS, respectively. Fig. 4 shows typical SEM images of selected samples. Representative samples of interest to the discussion here are listed in Table 1.

Fig. 4a shows the surface morphology of sample #30. A rather dense coating is evident on the surface, which contains a net of micro-cracks that may result either from hydrogen embrittlement or from residual stresses. Donten et al. [23] related similar cracking in amorphous Ni–W deposits mainly to high residual stresses and showed that by incorporation of Fe into an alloy deposited on iron-based substrates, this cracking could be eliminated, and both deposit toughness and adhesion could be improved. Eliaz [24] summarized several theories explaining the cracking in hard chromium electrodeposits. The residual stresses were related to defects that are incorporated in the coating, to volumetric contraction of the deposit, or to the way in which the chromium grains crystallize. In addition, the role of hydrogen in electrodeposition has been reviewed recently [3].

Table 2
Characteristics of selected samples.

Sample	Thickness (μm)	Rate (μm h^{-1})	FE (%)	Re (at.%)	Δm (mg)
23	16	16	57	60	45.3
30	4	12	39	66	10.2
32	25	15	36	71	47.0
33	12	12	11	93	8.8
56	22	22	36	85	27.8

Close examination of the surface shows that it consists of globular regions and either circular or quasi-circular domain borders. This indicates that no definite grain boundaries exist, consistent with an amorphous structure. The coating contained 66 a/o Re and was formed at FE = 39%. A surface morphology similar to that shown in Fig. 4a was observed in most of the as-received samples. In some cases, this morphology was the dominant one, while in other cases it was found only locally. A backscattered electrons image of the metallographic cross-section of this sample yielded a thickness value of approximately 4 μm obtained by plating for 20 min (cf. Table 2).

Fig. 4b shows the surface morphology of sample #32, plated under the same conditions, but for 100 min. A rather dense coating is seen, containing a net of larger micro-cracks. Craters with clusters at their bottoms can be seen in Fig. 4b. The FE (36%) and the composition of the deposit (71 a/o Re) were nearly the same as for the sample shown in Fig. 4a. The thickness of this sample, shown in Fig. 5a, is approximately 25 μm.

Fig. 4c shows the surface morphology of sample #54, for which the coating was conducted for one hour and the concentration of NH_4ReO_4 was increased to 50 mM, while all other plating parameters were not changed. The concentration of Re in the alloy was increased slightly to 76 a/o, but the FE remained nearly unchanged, at 38%. The surface morphology was smooth with no visible cracks. This sample can be considered the best of all samples shown in this manuscript, as far as the surface morphology is concerned, although it represents neither the highest Re content in the deposit nor the highest FE.

Fig. 4d shows the morphology of sample #56, for which the concentration of NH_4ReO_4 was further increased, to equal that of $Ni(NH_2SO_3)_2$, while all other parameters maintained unchanged. This yielded a relatively high Re-content in the deposit (85 a/o), yet maintaining nearly the same FE (36%). The surface morphology in Fig. 4d shows no micro-cracks, but flat rings were grown, either from or on top of the coating. These rings, which were observed only in this sample, cannot be explained at this stage.

Fig. 4e shows the surface morphology of sample #33. The concentrations of $Ni(NH_2SO_3)_2$ and NH_4ReO_4 were set equal, at a low

Table 1
Deposition conditions for selected samples.

Sample number	NH_4ReO_4 (mM)	$Ni(NH_2SO_3)_2$ (mM)	$C_6H_8O_7$ (mM)	Time (min)	
30	34	93	343	20	Fig. 4a
32	34	93	343	100	Figs. 4b and 5a
54	50	93	343	60	Fig. 4c
56	93	93	343	60	Fig. 4d
33	34	34	343	60	Fig. 4e
23	34	124	343	60	Figs. 4f and 5b
46	34	93	186	60	Fig. 4g
41	34	93	93	60	Fig. 4h

pH = 5.0 ± 0.1, T = 70.0 ± 0.1 °C, i = 50 mA cm^{-2}.

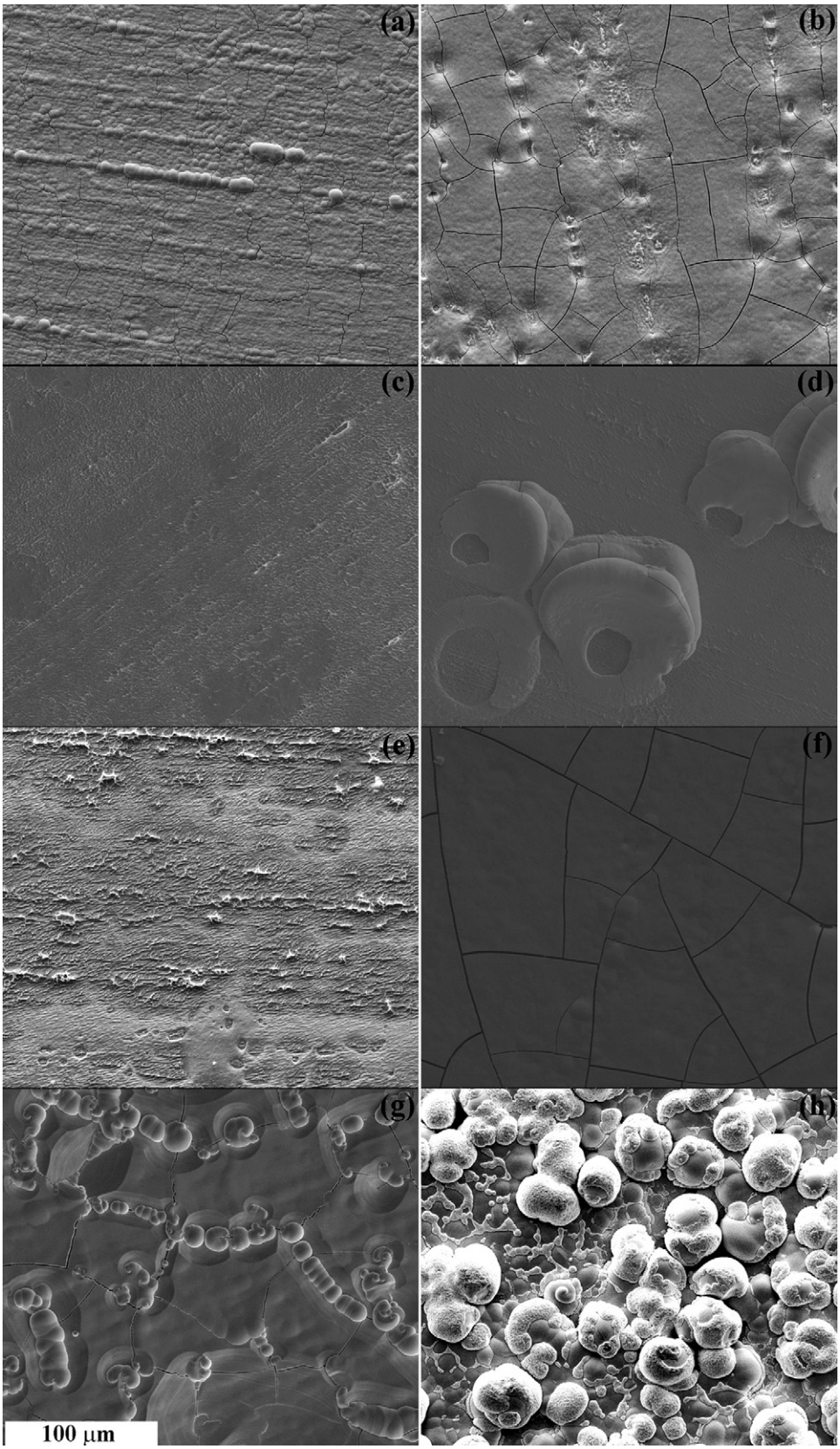

Fig. 4. Scanning electron microscope secondary electron images taken from eight Re–Ni coatings on copper substrates. Each image represents different process parameters (see Table 1 and text for more details). The length of the white scale bar corresponds to 100 μm.

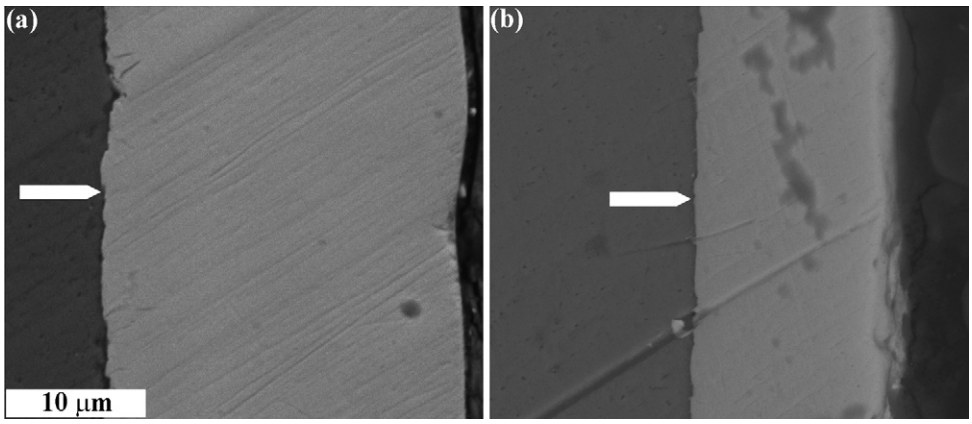

Fig. 5. ESEM backscattered electron images acquired from metallographic cross-sections of two Re–Ni alloys electrodeposited on copper substrates. Coating (see arrow) thickness is given in Table 2. The samples are: (a) #32, (b) #23 (see Table 1 for further details). The length of the white scale bar corresponds to 10 μm.

value of 34 mM. This yielded the highest Re-content in the deposit (93 a/o), but the FE was only 11%. It can be noticed that the surface morphology is irregular, but there seems to be no micro-cracks. A cross-section of this sample revealed a thickness of about 12 μm.

Fig. 4f demonstrates the surface morphology of sample #23, for which the concentration of $Ni(NH_2SO_3)_2$ was increased to 124 mM (3.65 times that of NH_4ReO_4). This change resulted in a decrease in the Re-content to 60 a/o, but the FE increased to 57%. The surface morphology is significantly different from that in Fig. 4e. A low density of relatively large cracks (ca. 0.5 μm wide) is seen. The hardness of this sample, as measured by the nano-indentation technique, was 928 ± 60 VHN (~68 HRC), which is higher than the typical range for commercially pure Re (265–765 VHN) [1,3]. A cross-section of this sample (Fig. 5b) reveals thickness of about 16 μm. Thus, it can be concluded that the higher nickel concentration in the bath yielded a thicker coating. This is the combined effect of increased FE and the much lower density of Ni compared to Re.

The next two surface morphologies revealed in Figs. 4g and h (samples #46 and #41, respectively) demonstrate the effect of decreasing the analytical concentration of $C_6H_8O_7$ while maintaining the other conditions as for Fig. 4a. The coatings contained 48.5 a/o and 24 a/o Re at FE of 74% and 76%, respectively. Globules tended to form when decreasing the analytical concentration of $C_6H_8O_7$, and the surface generally became less uniform.

4. Discussion

The mechanism of alloy deposition is a fascinating subject, particularly in the cases of anomalous or induced codeposition. In previous studies in our laboratory we proposed a mechanism of induced codeposition of W–Me alloys, where Me is an iron-group metal, say Ni. It is well known that pure W cannot be electrodeposited from aqueous solutions containing the tungstate ion, WO_4^{2-}, but its alloys with Ni (and some other transition metals) can be readily formed [3,25]. As a rule of thumb, the alloys formed were rich in Ni, the concentration of W being below 50 a/o [26–31]. This behavior was interpreted by assuming parallel paths for the deposition of Ni and observing an alloy with the composition of NiW.[2] It was argued that the precursor for Ni deposition could be its complex with citrate and/or NH_3. The codeposition of W with Ni was shown to result from the reaction

$$[(Ni)(Cit)]^{1-} + [(WO_4)(Cit)(H)]^{4-} \rightarrow [(Ni)(WO_4)(Cit)(H)]^{2-} + (Cit)^{3-} \quad (3)$$

It was concluded that the complex containing both metals is the precursor for deposition of the Ni–W alloy. The composition of the alloy is then determined by the ratio between the rate of deposition of Ni and W from this complex, and by the rate of the parallel deposition of Ni itself.

Rhenium is located next to W in the periodic table. Although the chemistry of these elements in solution is quite different, their most stable anions in aqueous solution, WO_4^{2-} and ReO_4^{-}, are isoelectronic. Thus, it was not unreasonable to assume, as a starting point for the study of electrodeposition of Re–Ni alloys, that there could be a similar induced codeposition of Re with Ni. However, it turned out that there are differences in the mechanism of deposition, as will be discussed below. To begin with, Re can be deposited from its aqueous solution, albeit at a rather low FE. Secondly, the concentration of Re in the alloy could readily exceed 50 a/o, even when the concentration of nickel in solution exceeded that of rhenium.

Considering Sample #30 in Table 1, we note that the ratio of molar concentrations of $Ni(NH_2SO_3)_2$ and NH_4ReO_4 was 2.74. Yet, Table 2 shows that the Ni–Re concentrations ratio in the alloy was 1:2. Moreover, for sample #33, the concentrations of Ni and Re in solution were equal, but the alloy contained 93 a/o Re. Comparing Fig. 2a and b, it is noted that increasing the concentration of rhenium in solution resulted in a slight decrease in the partial current density for deposition of Ni, whereas increasing the concentration of Ni in solution resulted in an increase of the partial current density for deposition of Re dramatically, by a factor of about five. Thus, the presence of nickel in solution is seen to catalyze the rate of Re deposition, but not vice versa. The Re content in the alloy decreased, of course, as seen in Fig. 2a, because there are parallel routes for deposition of Ni, unrelated to the presence of rhenium in solution, and the total rate of deposition of Ni increases even faster.

The effect of the concentration of nickel sulfamate in citrate baths was also investigated by Netherton and Holt [20]. It was found that, as the concentration of nickel sulfamate was increased, the Re content in the deposit decreased, while the FE increased to a maximum and then decreased somewhat.

In order to fully understand the behavior of complex processes, such as the deposition of W and Re alloys with Ni, it is necessary to consider the solution chemistry involved. In both cases we used citric acid as the complexing agent, which can form complexes not only with the positive Ni^{2+} ion, but also with the negative

[2] Under extreme condition of very large excess of the tungstate ion in solution, a phase corresponding to NiW_2, namely 67 a/o W, was detected. However, the corresponding FE was very low, of the order of 1% or less, making this process of little or no practical interest.

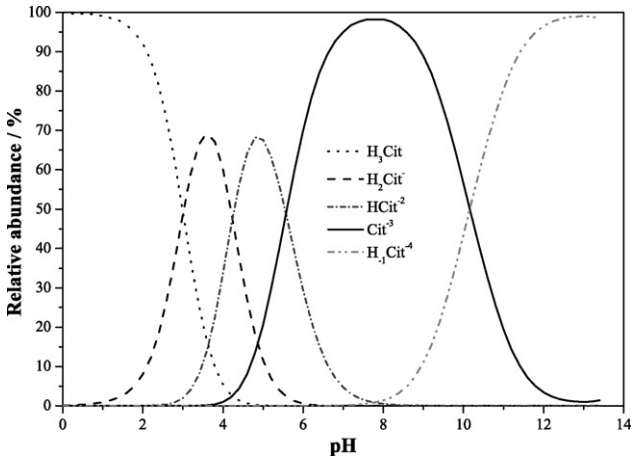

Fig. 6. The relative abundance (%) of citrate-containing species as a function of pH at 70 °C, 0.343 M analytical concentration of citric acid.

WO_4^{2-} and ReO_4^- ions. Fig. 6 shows the gradual deprotonation of citric acid. This figure was generated by the chemical equilibrium code ChemEQL version 3.010 [32]. The ionic product of water pK_w and the constant A in the Davies equation for activity corrections were calculated for $T = 70\,^\circ C$, using the equations given elsewhere [33], and values of 12.793 and 0.564811 $(dm^3\ mol^{-1})^{1/2}$ were obtained, respectively. It should be noted that the values $pK_1 = 3.13$, $pK_2 = 4.76$, $pK_3 = 6.39$ provided in the database of the computer code are slightly different than those used by two of us in previous publications [3]. However, the reaction of formation of $[H_{-1}Cit]^{4-}$ and the related $pK_4 = 10.82$ was added manually to the database. In spite of the slightly different input values used to construct Fig. 6, the output is similar to the figure reported in our previous study [3]. At pH = 8.0 ± 0.1, where most of our earlier work on W–Ni alloys was conducted, the predominant species (~98%) is the Cit^{3-} ion. In the present work on Re deposition the pH was set at 5.0 ± 0.1, where the three anions (H_2Cit^-, $HCit^{2-}$ and Cit^{3-}) exist at significant concentrations (11.6%, 67.7% and 20.7%, respectively), thus each of them could affect the solution chemistry.

In similar studies of deposition of W–Ni alloys it was shown that the FE increased as the concentration of nickel ions was increased, but decreased as the concentration of citrate ions was increased beyond the sum of concentrations of nickel and tungstate ions in solution [22]. The same behavior was found for the Re–Ni system in the present study, at pH = 5.0 ± 0.1.

Regarding the effect of pH in citrate-containing baths, Netherton and Holt [20] showed that it was not significant; the Re-content in the deposit remained nearly constant for pH values between 3 and 8, while the FE maintained a value of 90% from pH ≥ 4. In another work, the presence of citrate was found to markedly enhance the rate of reduction of perrhenate, through reversible formation of a 1:1 complex, $[(ReO_4)(H_2Cit)]^{2-}$ [34]. Previously, it was shown that baths containing citric acid yielded deposits with higher Re content compared to baths without citrate [20]. Furthermore, comparison of the behavior of alloy deposition from sulfate vs. ammoniacal citrate baths showed that the range of plating variables that resulted in deposits with high Re content at high FE was wider in the ammoniacal citrate baths than in the acid sulfate baths [18].

The complexes of Ni^{2+} with Cit^{3-} were given in previous publications [3,27,31]. The important thing to remember is that the rate of Ni deposition is expected to decrease in the order of $Ni^{2+} > NiCit > NiCit_2$, both at pH = 5.0 ± 0.1 and at pH = 8.0 ± 0.1. Thus, the ratio between the concentrations of citric acid, nickel and rhenium in solution is an important factor, controlling the rate of deposition, the FE and the composition of the alloy in the Re system (as also observed in the W system). In our previous work, the concentration of W in the alloy was found to increase with increasing concentration of citric acid up to a certain point, and then decreased. The increase was associated with the increased concentration of the precursor for deposition of the W–Ni complex (cf. Eq. (3)). However, too much citrate led to formation of the $[NiCit_2]^{4-}$ complex, thus decreasing the availability of $NiCit^-$, which is needed to form the precursor for the deposition of the alloy [3].

In the present study, the observations are more complex, as evident in Fig. 3a and b. Free Ni^{2+} and $[NiCit]^-$ are the predominant species, as long as the citrate-to-nickel ratio is Cit/Ni ≤ 1. As this ratio reaches unity, the concentration of free Ni^{2+} falls almost to zero. A further increase in the concentration of citrate leads to the formation of complexes such as $[(Ni)(Cit)(H)_n]^{n-4}$, where n equals 0, 1 or 2. These complexes can sequester the Ni^{2+} ion, thus inhibiting its reduction.

The perrhenate ion may form the complex $(ReO_4H_2Cit)^{2-}$ [34]. The relative concentration of this complex reaches a maximum of 96% at pH 5.5, and then decreases at higher pH values [35]. Consequently, at pH = 5.0 ± 0.1 and low concentration of citric acid, the predominant citrate complex is likely to be the perrhenate complex shown above. This can explain the dependence of the Re-content in the alloy on the Cit/Ni concentration ratio shown in Fig. 3a. Thus, when this molar ratio equals 0.4, most of the citrate is bound to the perrhenate ion in the complex, and the Ni^{2+} ion is free in solution. This allows reduction of nickel to its metallic form, which can then reduce the perrhenate ion chemically, via the reaction

$$7Ni^0 + 2(ReO_4H_2Cit)^{2-} + 16H^+ \rightarrow 7Ni^{2+} + 2Re^0 + 8H_2O + 2H_2Cit^- \quad (4)$$

Alternatively, the reduction could be only partial, according to the reaction:

$$Ni^0 + (ReO_4H_2Cit)^{2-} + 2H^+ \rightarrow Ni^{2+} + (ReO_3H_2Cit)^{2-} + H_2O \quad (5)$$

and the rhenate ion, ReO_3^- (which is less stable than the perrhenate ion), could be reduced electrochemically to metallic Re. This leads to a relatively high Re-content in the alloy at low citrate concentrations, as noticed in Fig. 3a, followed by a minimum in the range of Cit/Ni ≈ 0.8–1.25. The minimum observed is related to the drop of the concentration of Ni^{2+} to almost zero, which makes it more difficult to reduce Ni in order to allow one of the reactions, (4) or (5), to occur. The increase in the Re-content in the alloy at high citric acid concentration may be related to the formation of $[Ni(H_2Cit)_2]^0$ or $[Ni(HCit)_2]^{2-}$ species, which inhibit the parallel paths for deposition of Ni. It should be noted that, although most of the current passed may initially be consumed to reduce the Ni^{2+} ions in solution, a significant fraction of these ions may be regenerated via one of the two reactions shown above (cf. Eqs. (4) or (5)), instead of being incorporated in the deposited alloy, leading to a low apparent current density for reduction of Ni.

5. Conclusions

The factors affecting the electrodeposition of Re–Ni alloys, in particular the FE, the Re- content in the deposit and the surface morphology, were studied. Conditions for the formation of hard coatings with as high as 93 a/o Re and FE as high as 96%, for thickness up to 25 μm, were identified. The following relations were observed:

(i) As the perrhenate concentration in the bath was increased, the FE stayed quite constant, the Re-content and the partial current density for Re deposition increased, while the partial current density of Ni decreased slightly.
(ii) As the nickel ion concentration in the bath was increased, the FE and the partial current densities of both Ni and Re increased, whereas the Re content in the deposit decreased.

(iii) The citrate-to-nickel ratio in solution had significant effects on the characteristics of the coatings, including their surface morphology. Increasing this ratio resulted in a decrease in the FE and an increase in the Re-content, the latter occurring only at ratios of 1.0 and higher. A large excess of citric acid in solution caused an increase in the Re-content of the deposit, probably by blocking parallel paths for deposition of metallic nickel.

(iv) The bath composition had a significant effect on the surface morphology of the coating. In order to form a good coating quality, a large amount of citrate was needed.

(v) It is proposed that the mechanism by which addition of nickel sulfamate to the solution enhances the rate of deposition of Re is through a unique type of electroless plating, in which the reducing agent is metallic Ni formed in situ. Further experiments, possibly replacing Ni by other transition metals, should be performed, to confirm this proposed mechanism.

(vi) A mechanism of induced codeposition, such as that observed for Ni–W alloy deposition in our previous studies, was ruled out, because of the high Re-content of the alloy. Thus, as long as the Re-content in the alloy was <50 a/o, a mechanism involving a mixed metal complex (as in the case of Ni–W alloys) could be accepted, but in order to plate an alloy containing 80 or 90 a/o Re (which was achieved in this work) one would have to assume mixed metal complexes containing 4 and 9 perrhenate ions for each nickel ion, respectively, which is evidently unreasonable.

(vii) Although it is difficult to electroplate pure Re, the experiments reported here indicate that plating of alloys of Re with Ni (and probably other metals) can be performed and controlled to yield the desired properties of the deposit and in particular control the Re-content within wide limits, at acceptable values of the Faradaic efficiency.

Acknowledgements

The authors thank Z. Barkay for her help with the ESEM imaging of metallographic cross-sections, and M. Levenshtein for his help in the preparation of those samples. The authors are also thankful to CSM Instruments SA Ltd. (Switzerland) for their support in nano-indentation testing.

References

[1] Cambridge Engineering Selector (CES), ver 3.1, Granta Design Limited, Cambridge, United Kingdom, 2000.
[2] Rhenium, in: ASM Handbook, vol. 2, 10th ed., ASM International, Ohio, 1990, p. 1150.
[3] N. Eliaz, E. Gileadi, Induced codeposition of alloys of tungsten, molybdenum and rhenium with transition metals, in: C.G. Vayenas, R.E. White, M.E. Gamboa-Aldeco (Eds.), Modern Aspects of Electrochemistry, vol. 42, Springer, New York, 2008, p. 191 (Chapter 4).
[4] J.B. Lambert, in: ASM Handbook, vol. 2, 10th ed., ASM International, Ohio, 1990, p. 557.
[5] T. Grobstein, R. Titran, J.R. Stephens, ibid (1990) 581.
[6] S.J. Schneider, High temperature thruster technology for spacecraft propulsion, NASA technical memorandum 105348, IAF-91-254, 1991.
[7] M. Treska, L.W. Hobbs, J.P. Pemsler, in: S.B. Newcomb, J.A. Little (Eds.), Microscopy of Oxidation 3, Institute of Materials, London, 1997, p. 720.
[8] B.D. Reed, J.A. Biaglow, S.J. Schneider, Mater. Manuf. Processes 13 (1998) 757.
[9] J.J. Diaz, Potentials 15 (1996) 37.
[10] G.S. Root, J.G. Beach, in: B.W. Gonser (Ed.), Rhenium – Electrochemical Society Symposium, Elsevier, New York, 1962, p. 165.
[11] F. Lang, T. Narita, Intermetallics 15 (2007) 599.
[12] M. Fukumoto, Y. Matsumura, S. Hayashi, K. Sakamoto, A. Kasama, R. Tanaka, T. Narita, Oxid. Met. 60 (2003) 335.
[13] M. Pourbaix, Atlas of electrochemical equilibria in aqueous solutions, NACE, Texas (1974) 300.
[14] V.P. Greco, Plating 59 (1972) 115.
[15] S.I. Berezina, T.D. Keshner, V.T. Ivanov, Prot. Met. 28 (1992) 212.
[16] S.I. Berezina, T.D. Keshner, A.V. Chernova, Prot. Met. 29 (1993) 499.
[17] E.A. Efimov, T.V. Gerish, Prot. Met. 18 (1982) 782.
[18] H. Fukushima, T. Akiyama, M. Shimizu, K. Higashi, Met. Finish. 83 (1985) 37.
[19] A.E. Gavrikova, V.N. Varypeav, J. Appl. Chem. USSR 51 (1978) 2352.
[20] L.E. Netherton, M.L. Holt, J. Electrochem. Soc. 98 (1951) 106.
[21] S.I. Berezina, T.D. Keshnar, Yu.P. Khodyrev, V.P. Veselkov, Prot. Met. 29 (1993) 84.
[22] N. Eliaz, T.M. Sridhar, E. Gileadi, Electrochim. Acta 50 (2005) 2893.
[23] M. Donten, H. Cesiulis, Z. Stojek, Electrochim. Acta 45 (2000) 3389.
[24] N. Eliaz, J. Adv. Mater. 33 (2001) 27.
[25] O. Younes, E. Gileadi, Electrochem. Solid-State Lett. 3 (2000) 543.
[26] O. Younes, L. Zhu, Y. Rosenberg, Y. Shacham-Diamand, E. Gileadi, Langmuir (2001) 8270.
[27] O. Younes, E. Gileadi, J. Electrochem. Soc. 149 (2002) C100.
[28] L. Zhu, O. Younes, N. Ashkenasy, Y. Shacham-Diamand, E. Gileadi, Appl. Surf. Sci. 200 (2002) 1.
[29] O. Younes-Metzler, L. Zhu, E. Gileadi, Electrochim. Acta 48 (2003) 2551.
[30] T.M. Sridhar, N. Eliaz, E. Gileadi, Electrochem. Solid-State Lett. 8 (2005) 3.
[31] N. Eliaz, E. Gileadi, Proc. 209th Meeting, Electrochem. Soc., Denver, CO, USA, May 7–12 (2006); ECS Trans. 2 (2007) 337.
[32] B. Müller, Manual of ChemEQL (Version 3.0), Limnological Research Center EAWAG/ETH, Kastanienbaum, Switzerland, 2004.
[33] N. Eliaz, T.M. Sridhar, Cryst. Growth Des. 8 (2008) 3965.
[34] J.J. Vajo, D.A. Aikens, L. Ashley, D.E. Poeltl, R.A. Bailey, H.M. Clark, S.C. Bunce, Inorg. Chem. 20 (1981) 3328.
[35] M. Kohlickova, V. Jedinakova-Krizova, R. Konirova, J. Radioanal. Nucl. Chem. 242 (1999) 545.